

O. Russo¹, P. Roncioni², M. Marini³, S. Di Benedetto⁴, G. Ranuzzi⁵, S. Pizzurro⁶, M. Albano⁷

- ¹ Italian Aerospace Research Centre (CIRA), Via Maiorise snc, 81043 Capua, Italy, Email: <u>o.russo@cira.it</u> ² Italian Aerospace Research Centre (CIRA), Via Maiorise snc, 81043 Capua, Italy, Email: <u>p.roncioni@cira.it</u>
- ³ Italian Aerospace Research Centre (CIRA), Via Maiorise snc, 81043 Capua, Italy, Email: m.marini@cira.it
- ⁴ Italian Aerospace Research Centre (CIRA), Via Maiorise snc, 81043 Capua, Italy, Email: <u>s.dibenedetto@cira.it</u>
 - ⁵ Italian Space Agency (ASI), Via del Politecnico snc, 00133 Rome, Italy, Email: <u>giuliano.ranuzzi@asi.it</u>
 - ⁶ Italian Space Agency (ASI), Via del Politecnico snc, 00133 Rome, Italy, Email: simone.pizzurro@asi.it
 - ⁷ Italian Space Agency (ASI), Via del Politecnico snc, 00133 Rome, Italy, Email: marta.albano@asi.it

Abstract

The paper examines the propulsive and combustion performances of a hypersonic scramjet engine along with emission indexes for different species in the combustion process. Comprehensive Computational Fluid Dynamics (CFD) analyses cover the entire internal flow path (inlet, combustor and nozzle) for a flight-cruise configuration. Both power-off and power-on conditions are assessed using ANSYS FLUENT software with a steady Reynolds-Averaged Navier-Stokes (RANS) model and well-established air-hydrogen combustion kinetics schemes from existing literature. The impact of viscosity on engine performance is also assessed. The effect of equivalence ratio on combustion characteristics is evaluated by considering lean and rich mixture. The findings demonstrate a noteworthy enhancement in performance and the attainment of high combustion efficiency by the end of the engine cycle.

Keywords: Scramjet, hypersonic, CFD, supersonic combustion, emission indexes

1. Introduction

In 2021, CIRA (Italian Aerospace Research Center), through the "SPACE-IPERSONICA-TEC" project funded by the national program PRORA, took on the challenge of designing a scramjet hypersonic demonstrator named Scramjet Hypersonic Experimental Vehicle (SHEV). The project was co-funded by ASI (Italian Space Agency) in 2022 by means of the agreement "Research and technological development of a hypersonic demonstrator".

The paper outlines nose-to-tail Computational Fluid Dynamics (CFD) analyses conducted within the project, evaluating the impact of combustion kinetics chemical models, flight-cruise conditions, and flow models on aero-propulsive balance and emission indexes of chemical species.

The research demonstrates significant improvements in performance parameters such as combustion efficiency and kinetic and thermodynamic quantities. The ultimate goal is to establish the basis for further advancements in aerospace and hypersonic propulsion, with a specific focus on enhancing aero-propulsive performances and related national competences.

1.1 Scramjet configuration and mission description

The demonstrator design is based on the wave-rider concept, which aims to control shock waves generated during high-speed flight for generating high lift and reduced drag. The scramjet engine is

strictly integrated into the vehicle and is constituted by all the internal flow path, i.e. inlet, combustor and nozzle.

The design emphasizes an elliptical intake with contraction in the x-direction, as depicted in Figure 1, following the Busemann model for minimal total pressure losses. Also, the combustor has an elliptical section and it features a two-stage multi-struts injector system. The injection includes two semi-struts distributing 65% of hydrogen to outboard regions and a central full strut dispersing the remaining fuel into the combustor. The combustor is followed by the nozzle which transforms from an elliptical shape to one almost circular for improved expansion efficiency. The lack of boundary layer control devices is addressed with a diverging combustor geometry and staged injection of hydrogen gas.

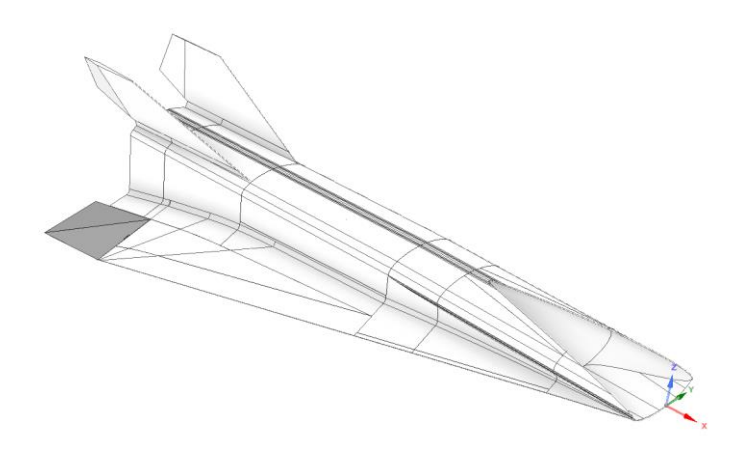


Figure 1 – SHEV external configuration.

The mission scenario features an air-launched approach, where an aircraft carrier releases (Sep I) a system (i.e., the payload) composed by the hypersonic demonstrator (SHEV) and the launch vehicle equipped with a solid fuel booster, designated to release the demonstrator at a certain altitude with a certain speed. The launch vehicle accelerates to the specified point and subsequently releases (Sep II) the hypersonic demonstrator for a 10-second scramjet-propelled phase in the experimental window. Computational Fluid Dynamics (CFD) analysis was conducted under the selected free stream conditions for the experimental window (Mach 6÷8 and altitude 27÷32 km), as depicted in Figure 2.

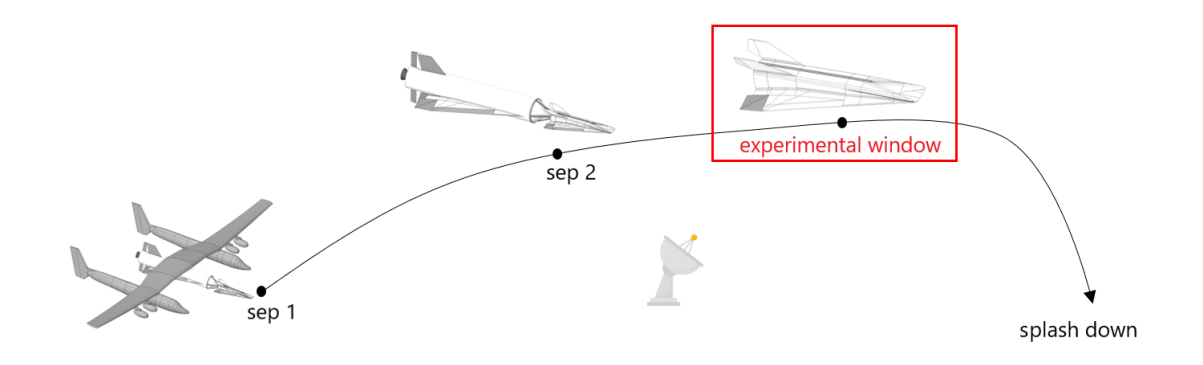


Figure 2 – Mission scenario.

2. Analysis

2.1 Numerical setting

Both full vehicle and internal flow path configurations have been considered to simulate the propulsive and chemical behavior. An unstructured grid composed of 7.6 million cells was employed on half configuration for the full vehicle as shown in Figure 3 while the internal flow path has 1.9 million cells for half configuration.

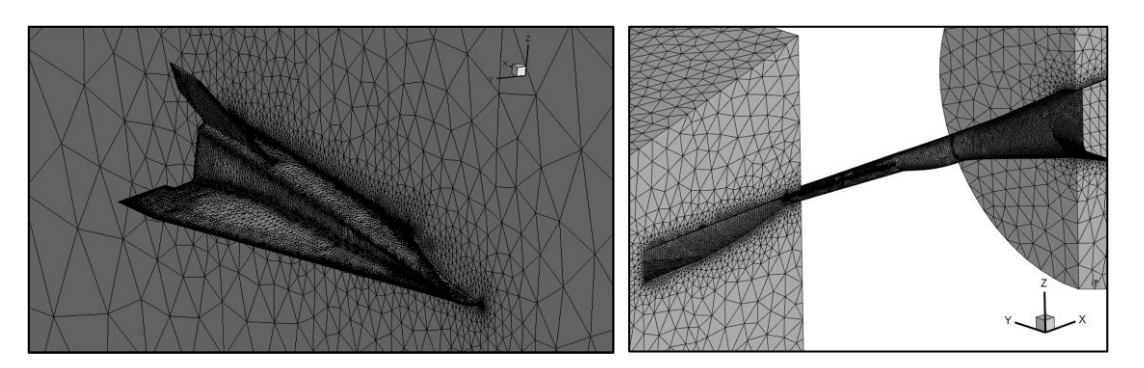


Figure 3 – Calculation grid for simulations.

Several quick preliminary CFD analyses, with inviscid flow model and in fuel-off condition, were performed on internal flow path configuration to assess the mass flow rate (MFR) of air entering the combustor at 0-deg angle of attack under various conditions chosen for the experimental window.



Figure 4 – Waterfall scheme.

The waterfall scheme presented in Figure 4 is very useful to explain the methodology used to derive the partitioned fuel to be injected into the combustor through a multi-stage strategy. The total mass flow rate of the hydrogen is immediately obtained by MFR of air, using stoichiometric condition (ER=1) and only a mono-step chemical scheme (eq. 1) for modelling air-hydrogen combustion.

$$2H_2 + O_2 + \frac{79}{21}N_2 \rightarrow 2H_2O + \frac{79}{21}N_2$$
 (1)

ER parameter represents the ratio between the fuel mass and air mass compared to the same ones evaluated in stoichiometric conditions. An ER greater than 1 indicates that the amount of fuel exceeds the oxidizer compared to the stoichiometric ratio. For air-hydrogen reaction the value of air-fuel ratio in stochiometric condition is equal to 0.029.

$$ER = \frac{\left(\frac{FUEL}{AIR}\right)}{\left(\frac{FUEL}{AIR}\right)_{st}}$$
 (2)

2.2 Fuel-ON analysis

In order to accelerate the CFD simulation convergence towards a steady solution, the reacting flow simulation starts from the converged solution of the cold flow where only the species equations are disabled. The comparison of fuel-off and fuel-on conditions with a mono-step chemical model (eq. 1) and inviscid flow field is displayed in Figure 5: as we can see the effect of combustion chemical

reaction takes place along the entire propulsion duct (combustion chamber and nozzle). The quantities represent the average values, integrated over different sections for some axial locations of the SHEV's propulsive flow path. Values are normalized with respect to free-stream conditions.

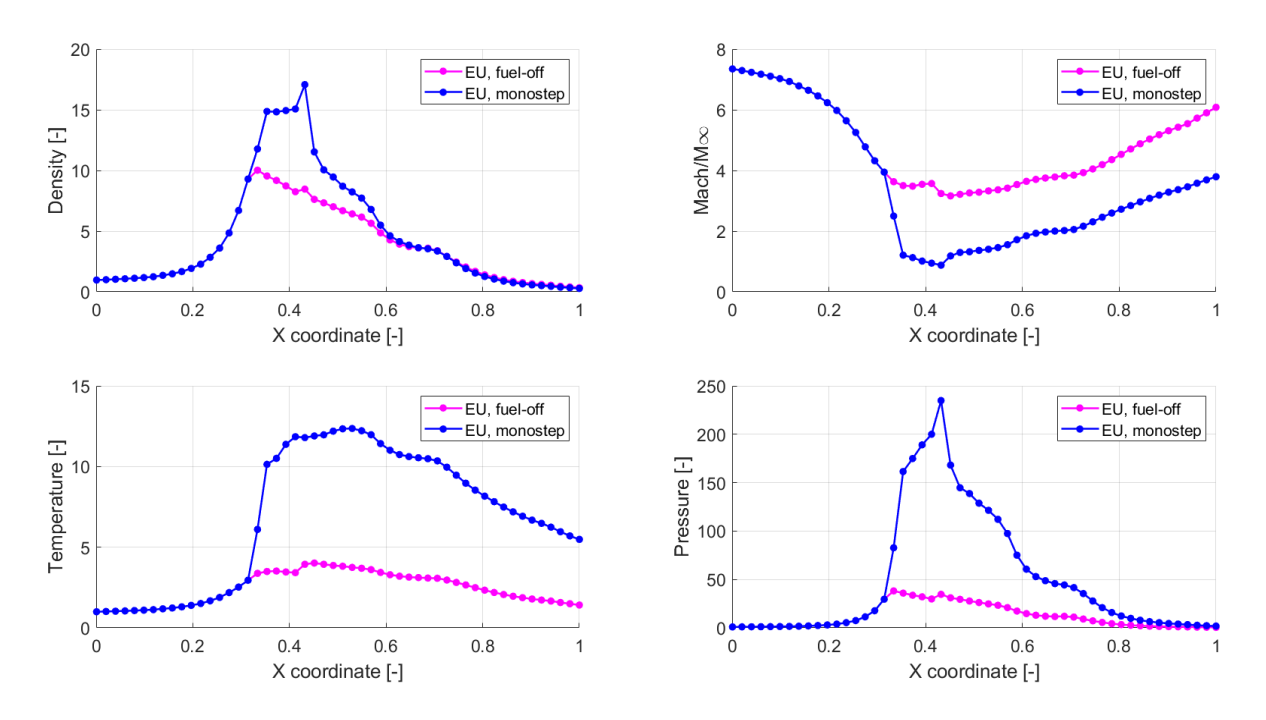


Figure 5 – Comparison of averaged mass fractions profiles for different species along the SHEV internal flow path at the same altitude. Fuel-OFF and Fuel-ON.

Steady Reynolds-Averaged Navier-Stokes, RANS, equations were then solved in fuel-on conditions. The turbulence of the flow was modelled with $k-\omega$ SST equations, whereas the combustion is described by using the finite-rate approach [7]. The finite-rate model employs the Arrhenius equation and chemical reaction details to compute the reaction rate. Main viscous results compared to inviscid results are reported in Figure 6 and Figure 7.

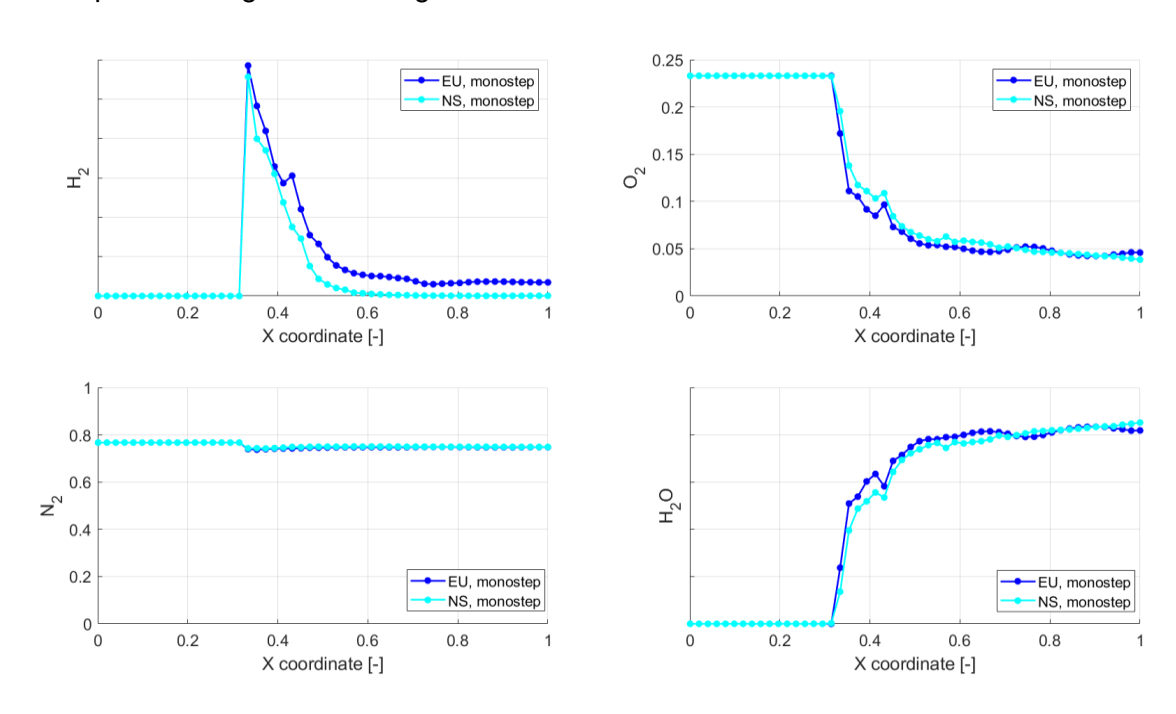


Figure 6 – Comparison of averaged mass fractions profiles for different species along the SHEV internal flowpath at the same altitude. Viscous (NS) and inviscid (EU) effect.

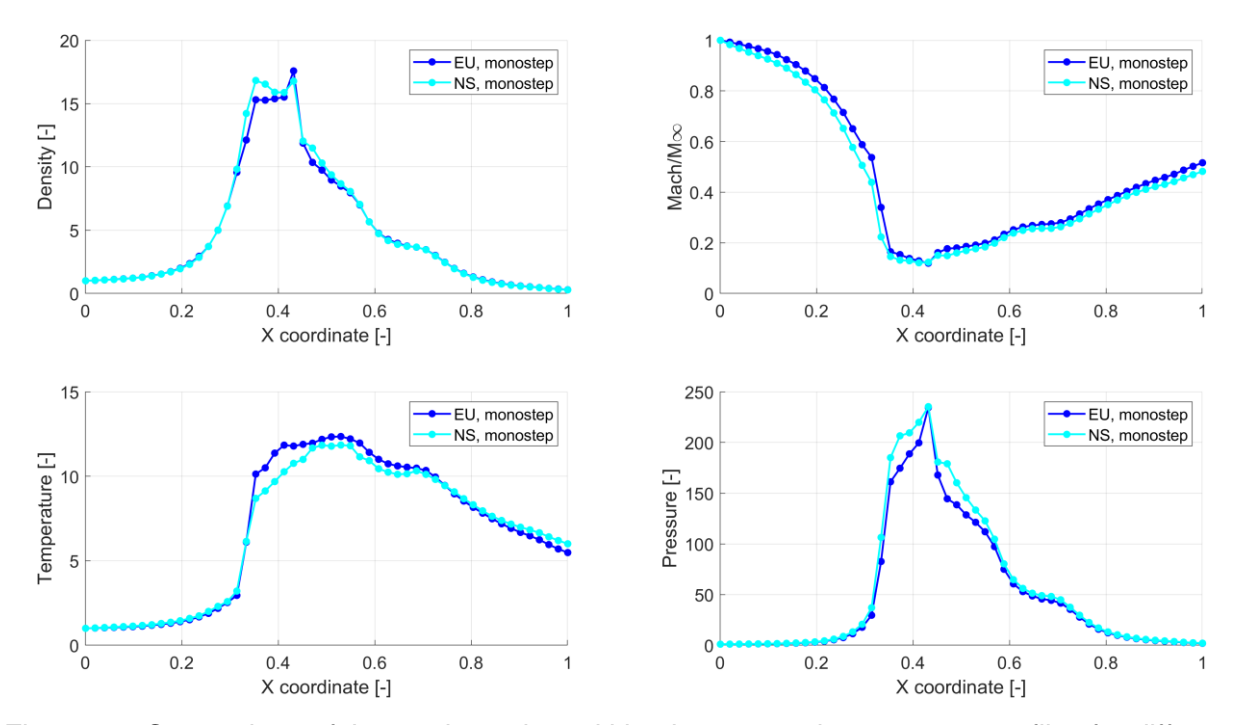


Figure 7 – Comparison of thermodynamic and kinetic averaged parameters profiles for different species along the SHEV internal flowpath at the same altitude. Viscous (NS) and inviscid (EU) effect.

The effect of viscosity does not seem to have a significant impact on the species involved in the single-step chemical model, as also evidenced by the H₂O averaged mass fraction in Figure 6. However, there is a slight effect of viscosity at the full-strut, where the injection of fuel appears dampened. In the zone near the wall, due to the presence of the boundary layer, the viscosity becomes even more important and leads to a local reduction of Mach number and temperature, and an increase of pressure, as observed in the distributions of the overall average values reported in Figure 7.

2.3 Multi-step reactions

To analyze in detail the behavior of the species involved in the combustion of the Air/GH₂ mixture, CFD simulations employed the Jachimowski reduced multistep chemical model. To avoid additional effects on comparison of combustion performance, the simulations were performed maintaining the finite-rate model, although the EDC model would have been more appropriate for the turbulence-chemical interaction [7] [8]. The reduced chemical model is less computationally expensive than the full model, in fact the reduced model includes only 7 chemical species (H₂, O₂, N₂, H₂O, H, O, OH) and involves 9 reversible species and chemical reactions of the elementary kinetic species.

R1)
$$H_2 + O_2 \leftrightarrow OH + OH$$

R2) $H + OH + M \leftrightarrow H2O + M$
R3) $H_2 + M \leftrightarrow H + H + M$
R4) $H + O_2 \leftrightarrow OH + O$
R5) $OH + H_2 \leftrightarrow H_2O + H$
R6) $O + H_2 \leftrightarrow OH + H$
R7) $OH + OH \leftrightarrow H_2O + O$
R8) $N_2 + M \leftrightarrow N + N + M$
R9) $O_2 + M \leftrightarrow O + O + M$

The three fundamental Zel'dovich reactions for the formation of NO (nitric oxide) species are adds in chemical model due their particular role in emissions, thus obtaining a total of 8 chemical species and

12 chemical reactions.

$$R10) N_2 + O \leftrightarrow NO + N$$

$$R11) O_2 + N \leftrightarrow NO + O$$

$$R12) N + OH \leftrightarrow NO + H$$

$$(4)$$

The Figure 8 details the NO concentration within the internal flow path of SHEV taking into account the Jachimowski reduced multistep chemical model with Zel'dovich reactions.

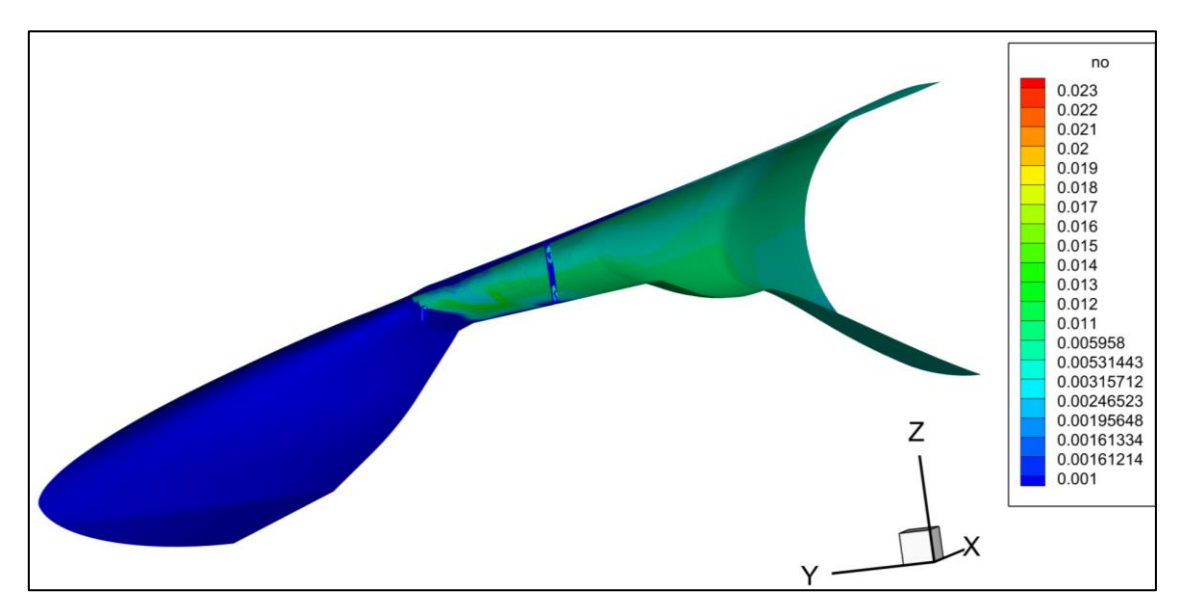


Figure 8 – Distribution of NO species inside the propulsion flow path internal surface.

Full comparisons of thermodynamic and kinetic averaged parameters are reported in the plots of Figure 9. The quantities are averaged values integrated over different sections at various axial locations of the SHEV.

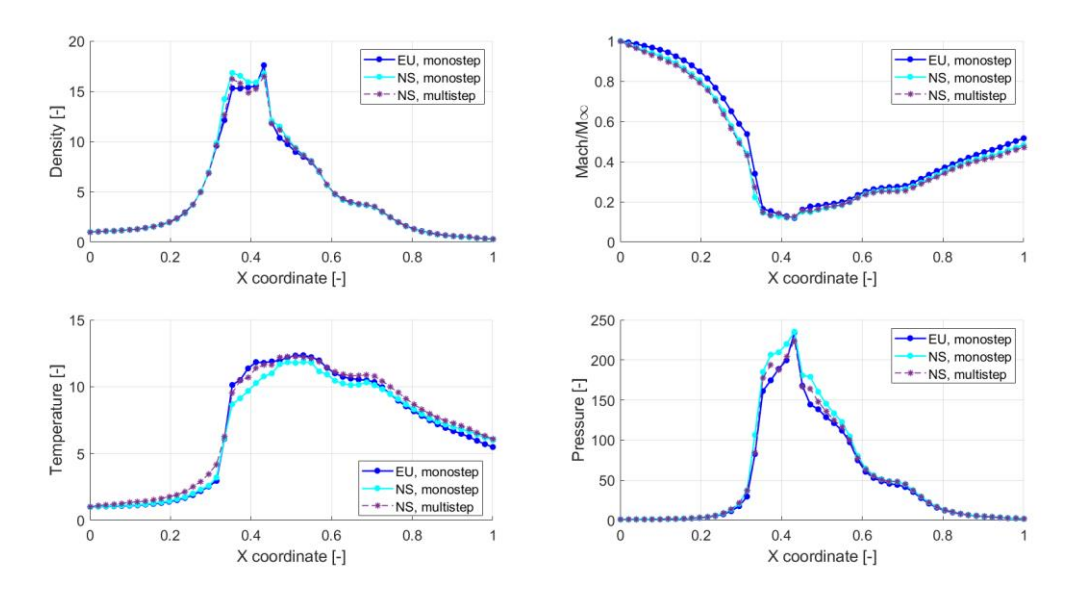


Figure 9 – Comparison of thermodynamic and kinetic averaged parameters for different species along the SHEV internal flowpath at the same altitude. Viscous (NS) effect. Monostep and multistep.

The Figure 9 does not reveal particular discrepancies between the distributions of the thermodynamic and kinetic parameters for multi-step and mono-step chemical reaction models, suggesting that these parameters are not so much influenced by the adoption of a more detailed multi-step chemical model.

However, the addition of heat to the supersonic flow in the combustion chamber reduces the Mach number and generates high pressure levels according to the Rayleigh flow theory. Notably, the thermal choking was not encountered in the analysis. In the nozzle region, the Mach number increases first slightly and then significantly due to the large section change in second part of the nozzle, thus realizing the conversion of thermal energy into kinetic energy as the flow expands (decreasing of temperature).

Figure 10 displayed the details of the two-stage injection strategy. On the left side of the figure, the semi-strut is shown, which injects (two of them) 65% of the hydrogen MFR through a nozzle at Mach=2 perpendicular to the main flow direction (it is aligned on x axis as the streamline shown). On the right side, there is a top view of the injection from one of two holes of the full-strut half configuration. This type of injection is advantageous for stabilizing the flame and improving the mixing with air flow.

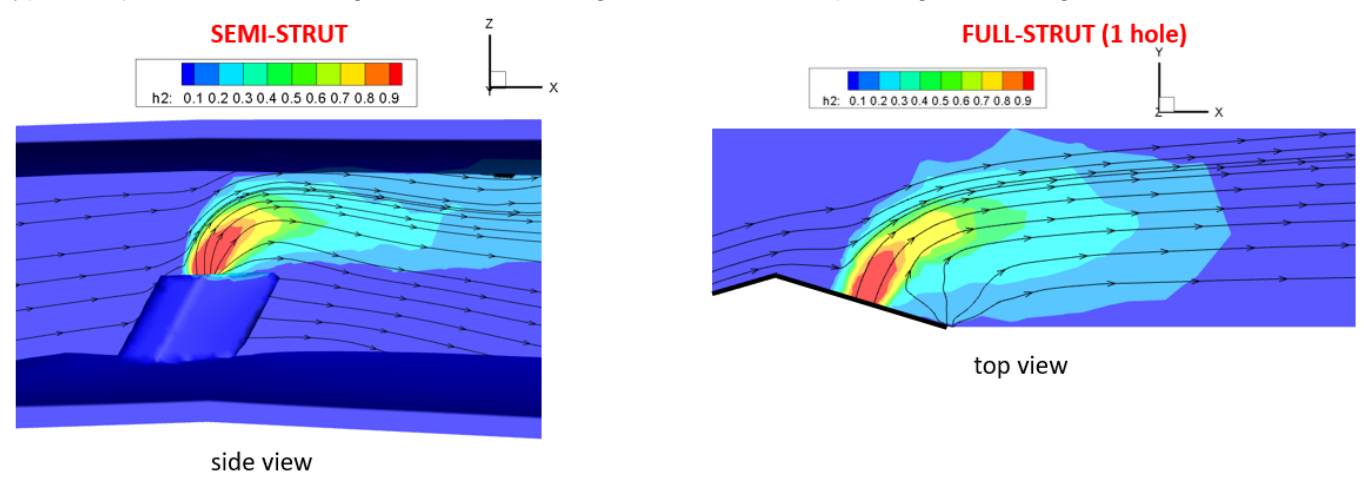


Figure 10 – Contours of hydrogen fuel mass fraction for semi struts (left, lateral view) and one hole of the full strut (right, top view).

As depicted in Figure 11 (not the full combustor is shown) the semi-strut is positioned near the combustor wall, while the full-strut is located downstream in the symmetry plane. The consumption of fuel injected by the full-strut is very quick and it is evident also from the small region observed by the hydrogen iso-surface of Figure 11. This phenomenon motivates the choice to divide the hydrogen fuel MFR differently between the semi-strut and full-strut, to also prevent combustion from taking place in the nozzle and completing outside the engine due to the short residence times of the locally supersonic flow.

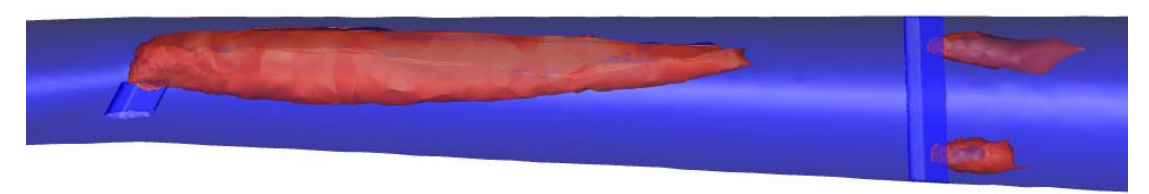


Figure 11 – Contour of iso-surface of constant hydrogen mass fraction (y_{H_2} =0.05).

The comparison of section-averaged mass fractions of species involved in multi-step reactions at the two different altitudes, named A and B, is considered and results are shown in Figure 12. The B altitude is higher than the A altitude, causing a difference in air mass flow rate due to the decrease of the free-stream quantities like temperature, pressure and density even though the composition of the air remains unchanged. Due to the lower temperature of altitude B, the chemical kinetics slows down resulting in a lower production of chemical species during the combustion process and this is clearly highlighted by the comparison of mass fractions of species at the two different altitudes. The trends are however preserved as showed in Figure 12, in fact, in correspondence with the decrease in the mass fractions of the O and N species, there is an increase in the mass fraction of nitric oxide. Notably, the averaged value of NO mass fraction is larger for the A altitude due to the elevated free-stream temperature. The mass fraction of water starts to rise when the hydrogen is injected and reaches flat when the fuel is completely consumed.

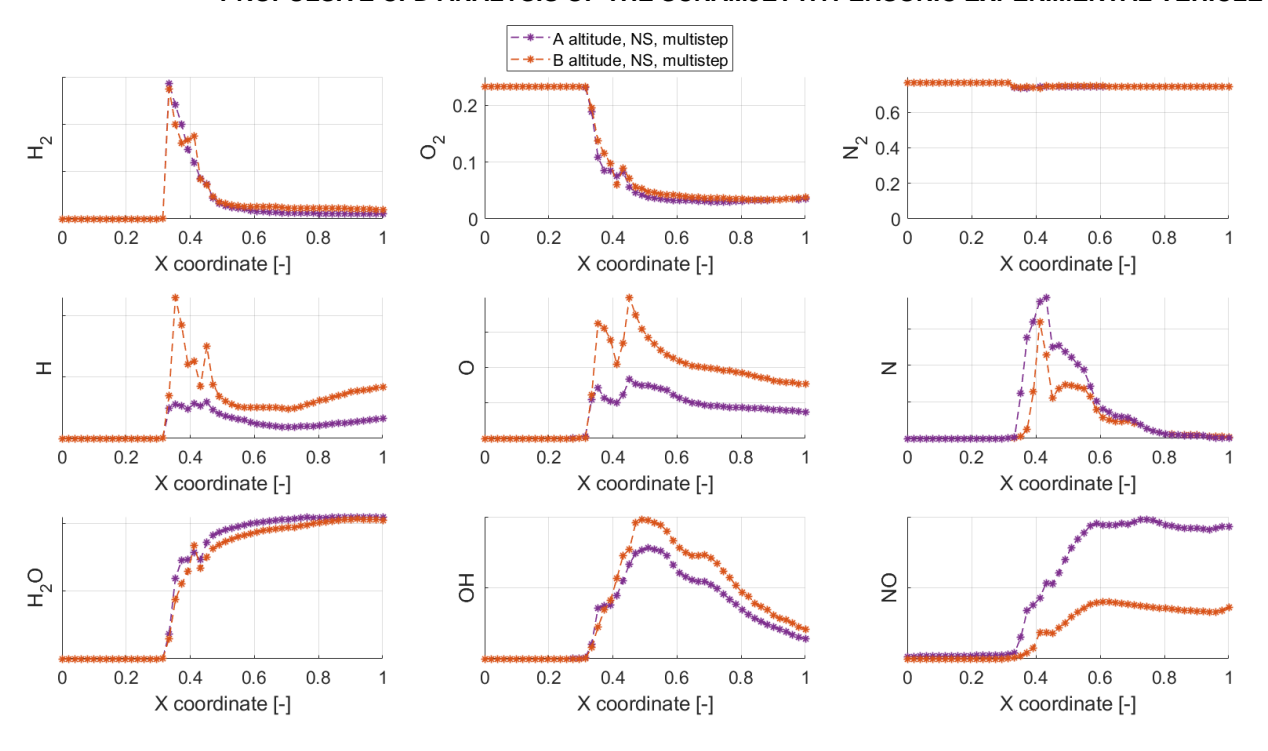


Figure 12 – Comparison of averaged mass fractions profiles for different species along the SHEV internal flowpath. Viscous (NS) effect. A altitude and B altitude.

2.4 Equivalence ratio effects

The equivalence ratio, ER, has already been defined in eq. 2 and is useful to evaluate the fuel-air ratio. In stoichiometric condition ER is equal to 1.0. A rich mixture is characterized by an ER greater than 1, while for a lean mixture ER is lower than 1. Figure 13 shows fuel injection with a desired global ER equal to 1, although locally varies. In fact, at the injection of hydrogen from the semi-strut the mixture is rich in fuel as is to be expected. The ER value gradually attenuates upstream of the semi-strut due to mixing with the air present in the duct.

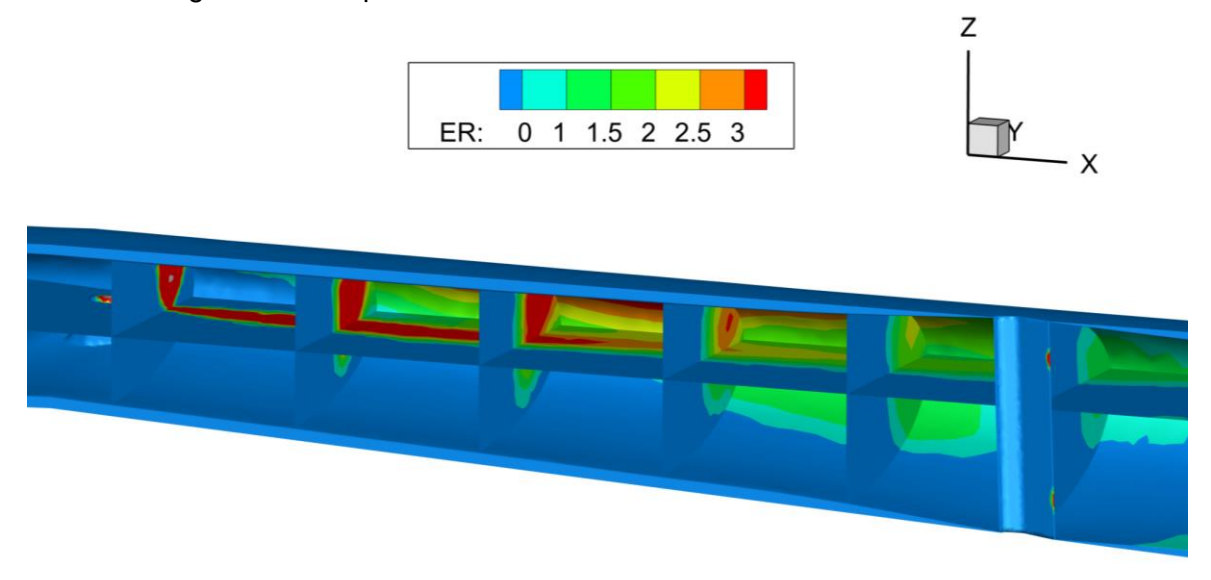


Figure 13 – Trend of fuel-air ratio in combustor engine at several slice locations.

The effect of the equivalence ratio on thrust is displayed in Figure 14. The thrust values are normalized respected to thrust value computed at ER=1 with mono-step chemical model by neglecting the viscous effect. A decrease in thrust is observed in Figure 14 when switching from a single-step to a multi-step combustion kinetics chemical model at the same ER, and this because part of energy involves also

the formation of NO molecules. Thrust with the mono-step chemical model (IFP) increases by approximately 25% when ER increases from 1 to 1.4.

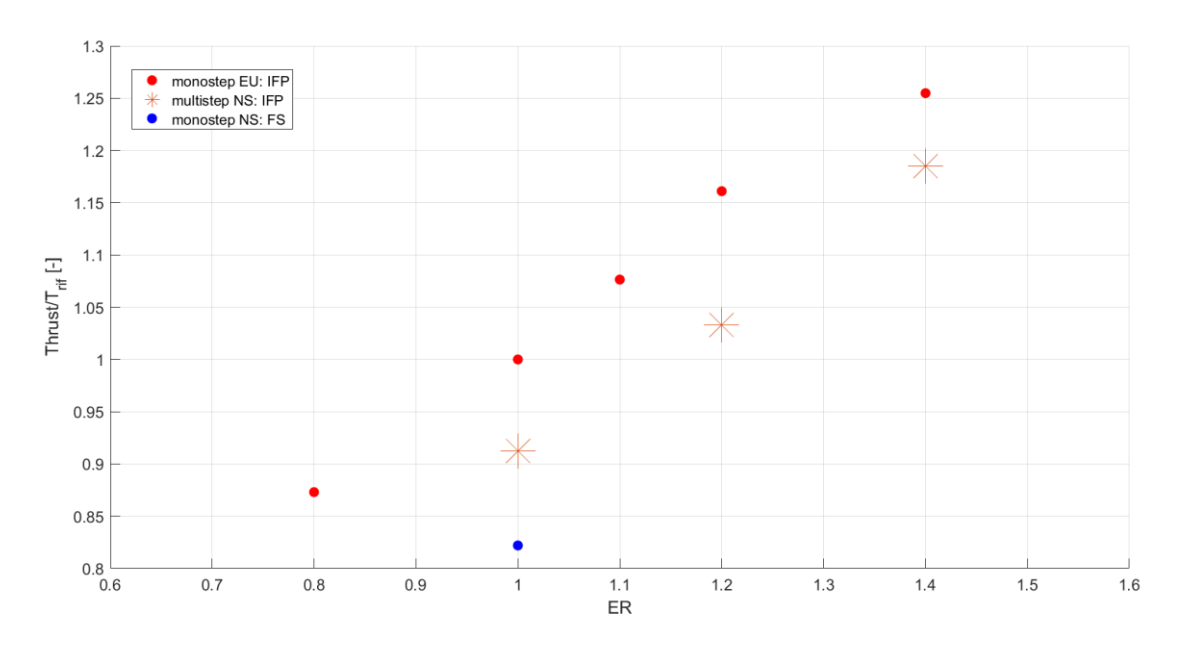


Figure 14 – Comparison of dimensionless thrust. IFP (internal flow path) and FS (full SHEV).

Due to limited computational resources the full configuration of 7.6 million cells is only computed with a mono-step reaction chemical model and with TCI (Turbulence Chemistry Interaction) effect at ER=1, as reported in Figure 14. The Internal Flow Path includes only scramjet components such as the open inlet, the combustor and the nozzle. On the other hand, Full SHEV includes not only the internal flow path but also the external parts of the demonstrator. As expected, the flow that enters into scramjet is affected by interference from external components and this results in a decrease in thrust. The choice of the minimum value of ER must at least guarantee that the aero-propulsive balance, evaluated as T-D (Thrust minus Drag), is greater than zero.

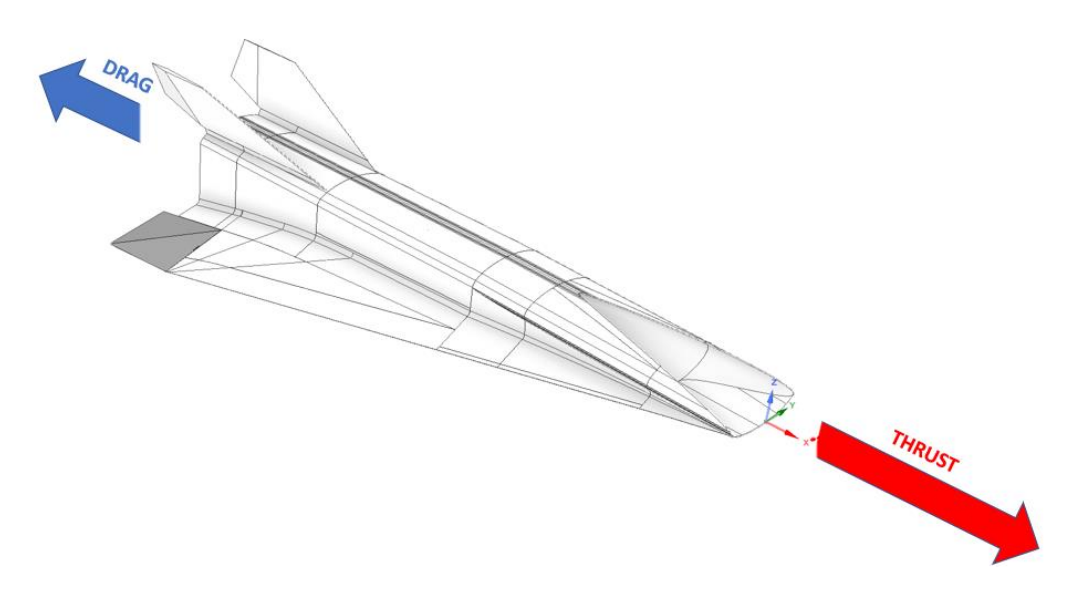


Figure 15 – Aero-propulsive balance scheme.

Figure 16 presents the relationship between the mass fractions of the involved species and the equivalence ratio for air-hydrogen combustion. A rich fuel mixture causes a reduction in the molecular fraction of oxygen and an increase in water vapor which is the only product (NO production reactions are not considered in the mono-step chemical model).

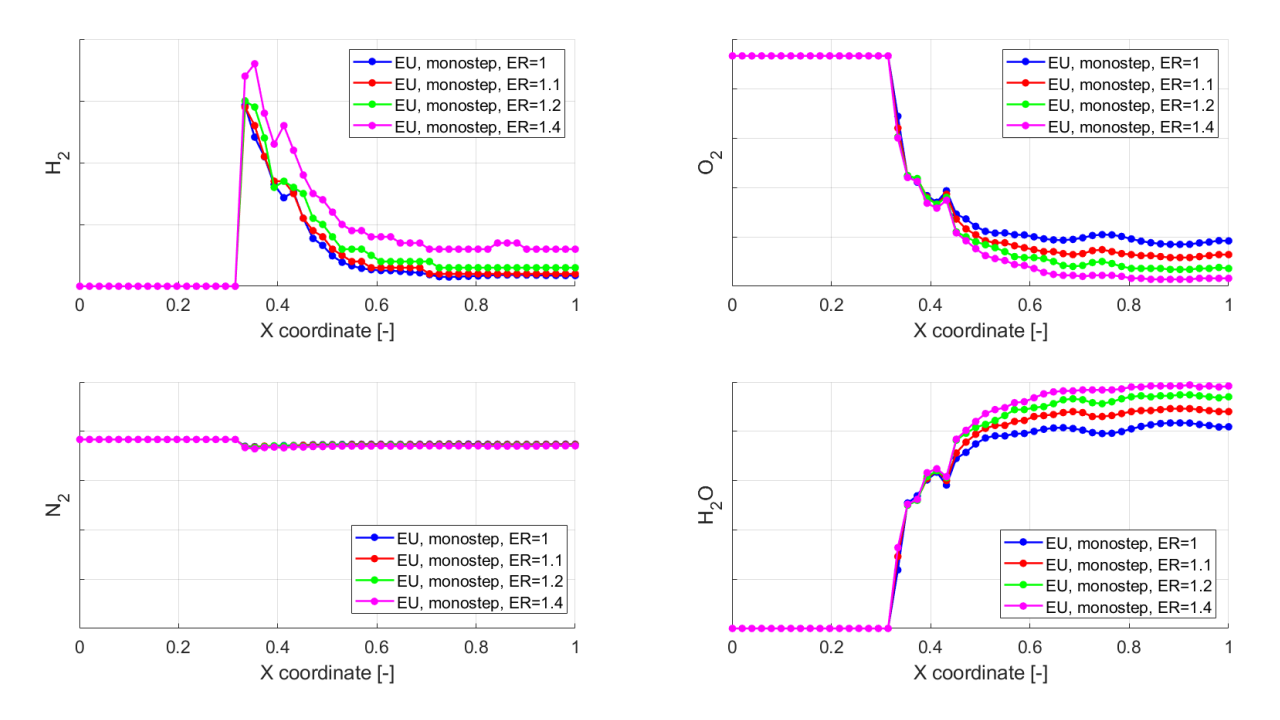


Figure 16 – Comparison of mass fraction species along internal flow path of SHEV at various ER. Mono-step chemical model.

2.5 Combustion efficiency

An important design parameter for the SHEV is combustion efficiency, η_c , defined as:

$$\eta_{c} = \frac{m_{\text{H}_{2 \text{ injected}}} - m_{\text{H}_{2}}}{m_{\text{H}_{2 \text{ injected}}}} = \frac{m_{\text{H}_{2 \text{ burned}}}}{m_{\text{H}_{2 \text{ injected}}}}$$
(5)

The viscosity does not significantly affect the engine performance in terms of its overall thrust thanks to greater mixing of the air-fuel mixture that leads to an improvement of the combustion efficiency so counteracting the negative effect of viscosity as shown in Figure 17. Furthermore, the same figure illustrates how the combustion efficiencies, for the multi-step reactions modelling, are lower than in the mono-step reaction because, unlike the latter, in which the energy released by the chemical reaction is used exclusively for the formation of H_2O , in the multi-stage reactions a portion of the energy is also used for the formation of NO. The available time for the chemical reaction is extremely limited due to the rapid flow velocity, and as a result, the combustion is completed inside the very early portion of the nozzle, where combustion efficiency reaches a plateau.

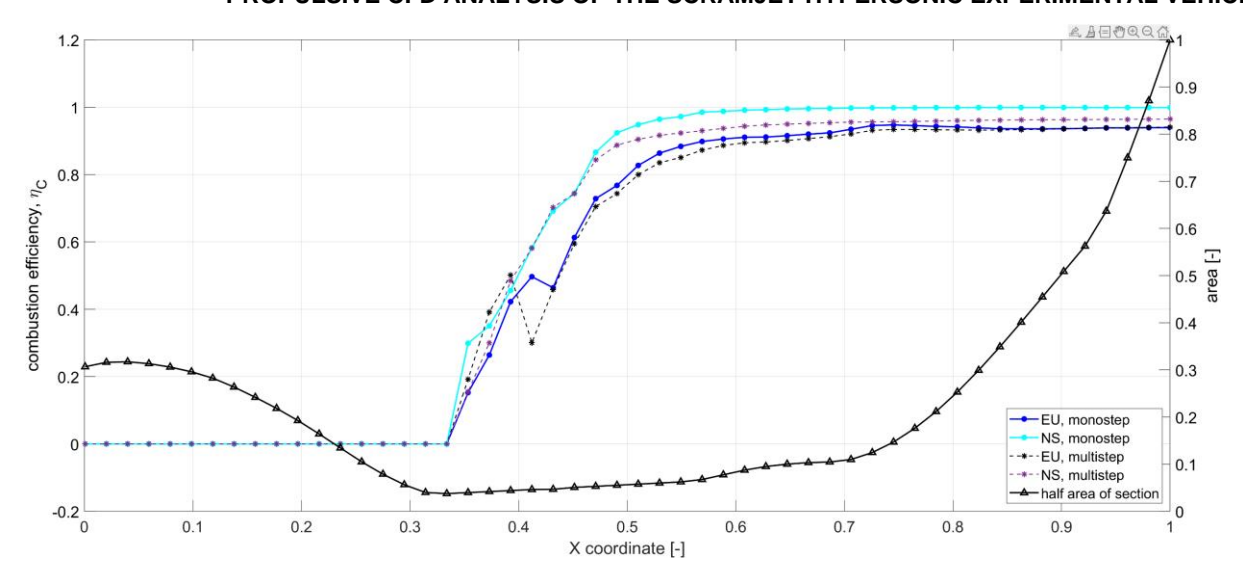


Figure 17 – Comparison of combustion efficiency along internal flow path of SHEV. Viscous (NS) and inviscid (EU) effect. Multi-step chemical model.

2.6 Comparison with LAPCAT-II project

The CFD analyses of SHEV combustor's performance are compared with the results of the LAPCAT-II project full-scale hypersonic cruiser MR2.4 [9], these latter also supported by experimental test campaigns. In particular, the following figure shows the comparison of the combustion efficiency of the two combustors versus the axial coordinate normalized with respect to combustor's length. An important information obtained from the comparison concerns the efficiency value. In fact, the predicted values for the two combustors are very close to one despite being equipped with a different configuration of strut-injectors.

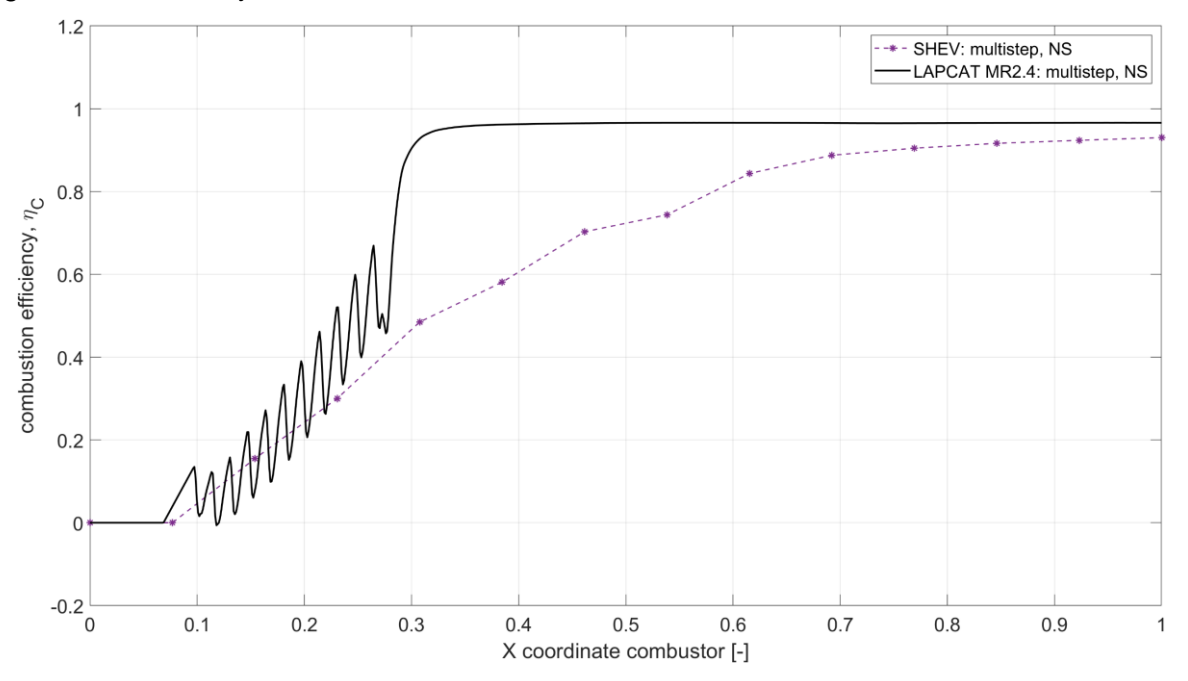


Figure 18 – Comparison of combustion efficiency along combustor conduct. Viscous effect (NS).

Multi-step chemical model. SHEV vs. LAPCAT-II MR2.4.

The scramjet combustor in the LAPCAT-II MR2.4 vehicle was equipped with a counter-V array of strut-injectors [8], as the oscillations of hydrogen mass-fraction clearly show in Figure 19, whilst the injection of fuel in the SHEV combustor is multi-staged and takes place in two different places (two symmetrical semi-struts at the beginning of combustor and a central full-strut located downstream).

As shown in the same figure and confirmed by previous results, the viscous effects and consequent fuel mixing have dampened a lot the predicted values in terms of section-averaged distributions.

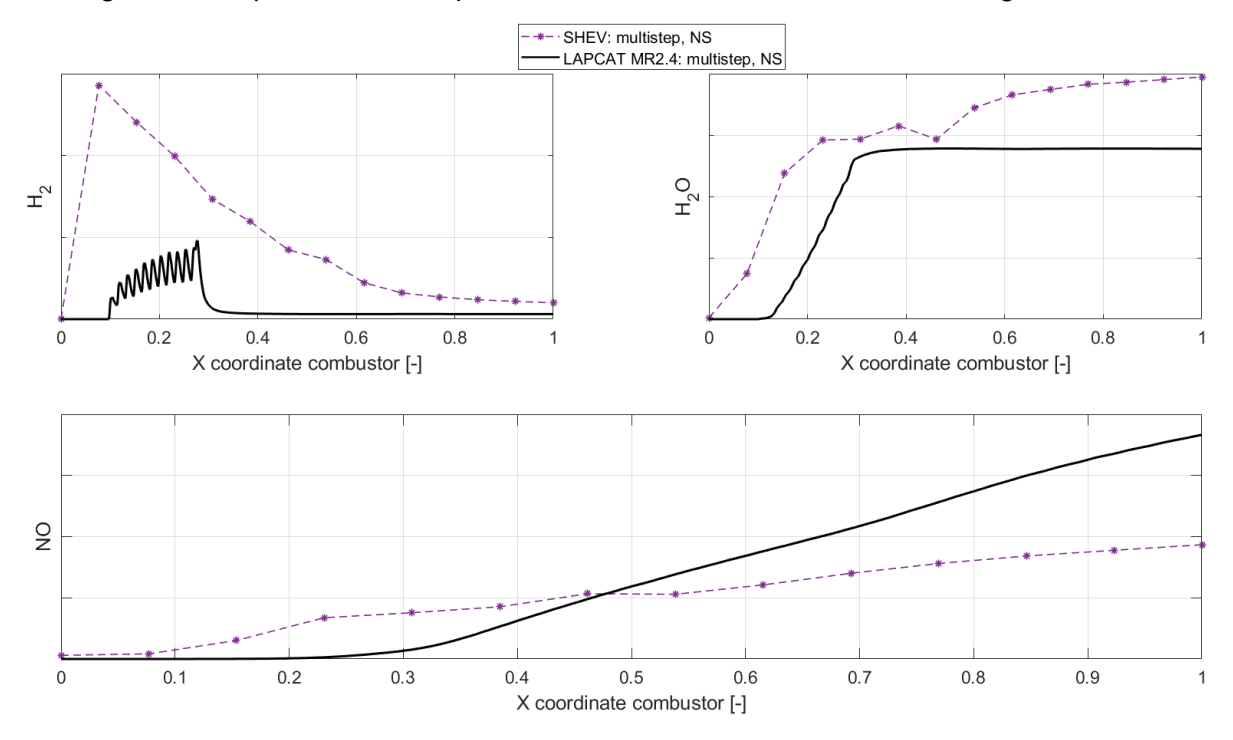


Figure 19 – Comparison of averaged mass fractions profiles for different species along combustor conduct. Viscous effect (NS). Multi-step chemical model. SHEV vs. LAPCAT-II MR2.4

3. Conclusions

In this work the nose-to-tail CFD activities of the SHEV's scramjet propulsive flow path is presented demonstrating that the combustion efficiently takes places in the combustor thus allowing a positive aero-propulsive balance.

A broad range of equivalence ratio is analyzed at the same operating conditions but a particular attention is focused on the stoichiometric condition, characterized by ER equal to 1, which allows studying the fuel consumption among the semi-strut and full-strut. The semi-strut normalwise injection is combined with the full-strut transverse fuel injection, this least acts as a blunt body and generates a detached shock wave that aids stability and mixing of the Air/H2 mixture. The implementation of Jachimowski's multi-step air-hydrogen combustion model in CFD simulations has enabled a more detailed understanding of the behavior of the species involved in the process, particularly in terms of nitric oxide thanks to the Zel'dovich reaction mechanism for NO generation. Activation of the viscosity model for CFD analysis with multi-step reactions, although very computationally expensive, is crucial for a realistic prediction of the phenomenology and indicated a combustion efficiency close to unity at the end of the combustor. This value is also confirmed by the comparison of the results with the predicted data of the MR2.4 full-scale hypersonic vehicle, studied in depth in the LAPCAT-II project. Furthermore, the effect of equivalent ratio on thrust is evaluated showing a reduction in thrust value for the multi-phase air-hydrogen combustion model due to the involvement of multiple species during the combustion process. However, a full configuration has a lower thrust value due to the interference of the external regions of the SHEV with the internal flow path.

Future activities will involve the analysis of the complete vehicle with a multi-stage air-hydrogen combustion model.

Acknowledgements

The work has been co-funded by Italian Space Agency and CIRA ScPA in the frame of the agreement nr. 2022-13-HH.0; CUP F43D22000410005.

Contact Author Email Address

The contact author email address is o.russo@cira.it

Copyright Statement

The authors confirm that they, and/or their company or organization, hold copyright on all of the original material included in this paper. The authors also confirm that they have obtained permission, from the copyright holder of any third party material included in this paper, to publish it as part of their paper. The authors confirm that they give permission, or have obtained permission from the copyright holder of this paper, for the publication and distribution of this paper as part of the ICAS proceedings or as individual off-prints from the proceedings.

References

- [1] J. Steelant et al.: Conceptual Design of the High-Speed Propelled Experimental Flight Test Vehicle HEXAFLY". AIAA-2015-3539. 20th AIAA International Space Planes and Hypersonic Systems and Technologies Conference, Glasgow, Scotland, U.K. July 6-9, 2015.
- [2] Di Benedetto S., Di Donato M.P., Schettino A., Scigliano R., Nebula F., Morani G., Cristillo D., Marini M., Cardone S., Steelant J., Villace V.: The high-speed experimental flight test vehicle of HEXAFLY INT: a multidisciplinary design. CEAS Space Journal. (2021). DOI: 10.1007/s12567-020-00341-5.
- [3] Viola N., Fusaro R., Saracoglu B., Schram C., Grewe V., Martinez J., Marini M., Hernandez S., Lammers K., Vincent A., Hauglustaine D., Liebhardt B., Linke F., Fureby C.: Main Challenges and Goals of the H2020 STRATOFLY Project. Aerotecnica Missili & Spazio. (2021). 100:95–110, Published online: 29 May 2021, https://doi.org/10.1007/s42496-021-00082-6
- [4] Viola N., Roncioni P., Gori O., Fusaro R.: Aerodynamic Characterization of Hypersonic Transportation Systems and Its Impact on Mission Analysis. MDPI-Energies. 16 June 2021. https://doi.org/10.3390/en14123580.
- [5] Mack A., Steelant J., Adirim H., Lentsch A., Marini M., Pilz N.: FAST20XX: Achievements on European Suborbital Space Flight. 7th European Symposium on Aerothermodynamics. Brugge. Belgium. May 2011.
- [6] Marini M., Saccone G., Chemical Kinetic Analysis of High-Pressure Hydrogen Ignition and Combustion toward Green Aviation. MDPI-aerospace. 25 January 2024.
- [7] Shizhuo Huang, Qian Chen, Yuwei Cheng, Jinyu Xian and Zhengqi Ta, Supersonic Combustion Modeling and Simulation on Genera Platforms, 7 July 2022, MDPI aerospace, doi.org/10.3390/aerospace9070366
- [8] Saccone G., Natale P., Marini M., Cutrone L., Hydrogen/Air Supersonic Combustion Modelling and Validation for Scramjet Applications, Journal of Fluid Flow, Heat and Mass Transfer (JFFHMT), doi: 10.11159/jffhmt.2022.017.
- [9] Roncioni P., Natale P., Marini M., Langener T., Steelant J., Numerical simulations and performance assessment of a scramjet powered cruise vehicle at Mach 8. Aerospace Science and Technology. Volume 42. 2015. ISSN 1270-9638.